J. Mt. Sci. (2014) 11(6): 1478-1490
DOI: 10.1007/s11629-014-3041-1
e-mail: jms@imde.ac.cn
http://jms.imde.ac.cn

A Comparison of Conventional and Shear-Rate Dependent Mohr-Coulomb Models for Simulating Landslides

LIANG Dong-fang[1,2]*, HE Xu-zhen[2]

1 MOE Key Laboratory of Hydrodynamics, Shanghai Jiao Tong University, Shanghai 200240, China

2 Department of Engineering, University of Cambridge, Trumpington Street, Cambridge CB2 1PZ, UK

**Corresponding author, e-mail: d.liang@sjtu.edu.cn; Tel.: +86 21 34204472; 2nd author, e-mail: xh248@cam.ac.uk; Tel: +44 1223 761262*

Citation: Liang DF, He XZ (2014) A comparison of conventional and shear-rate dependent Mohr-Coulomb models for simulating landslides. Journal of Mountain Science 11(6). DOI: 10.1007/s11629-014-3041-1

Abstract: Landslides may cause many fatalities and heavy economic losses, so it is vital to understand their mechanics so as to take appropriate measures to mitigate their risk. Phenomenally, the loose soil behaves like frictional material in most circumstances, so Mohr-Coulomb type equations are often used to describe their movement. However, these models generally do not consider the influence of the shear-rate on the Mohr-Coulomb friction angle, so the shear-rate dependence effect on the soil flow and landslide runout is not well understood. This paper reports on an application of the incompressible Smoothed Particle Hydrodynamics (SPH) method to the dynamics of dry granular assemblies. The traditional model with a constant friction angle is compared with the modified Mohr-Coulomb model with a variable friction angle related to the shear-rate. It is found that the shear-rate dependence effect is negligible for shallow granular flows along mild slopes. With steeper slopes of the ground and larger aspect ratios of the initial soil column, the rate-dependence effect becomes more important.

Keywords: Landslides; Granular flows; Mohr-Coulomb model; Smoothed Particle Hydrodynamics

Introduction

Landslides are a geological hazard that claims lives and threatens infrastructure in mountainous regions. They often happen suddenly and move too fast to enact mitigation measures once they are initiated. In addition, they often accompany other types of natural hazards like floods, earthquakes and volcanic eruptions. Consequently, a quantitative study of landslides is necessary in developing guidelines for land-use management and stabilizing steep slopes in mountainous cities.

The Bingham type model was first proposed based on the phenomena that loose material has both the properties of viscous fluids and plastic solids,. However, debris mass is a two-phase mixture consisting of the soil skeleton and fluids in the pores. In the recent literature, the behaviour of the soil skeleton and the interstitial fluids is often modelled separately, adopting the concept of the effective stress principle and consolidation equations based on Darcy's law.

With regard to the model for the soil skeleton, the Mohr–Coulomb failure criterion is an important physical principle. Savage and Hutter (1989) incorporated the Mohr–Coulomb model with depth averaged techniques to construct a set of reduced equations for dry granular flows containing only two free parameters: internal friction angle and bed friction angle. These equations have been successfully used for predicting dry granular motion over complex basal

Received: 27 February 2014
Accepted: 6 May 2014

topography in the laboratory and also the real-world debris flows.

However, the shear-rate dependent characteristic of the Mohr–Coulomb friction angle is generally not considered in the existing models for predicting dry granular avalanches, hence the influence of this effect on the runout has not been well understood. The Mohr-Coulomb model originates from the observation of shearing experiments under a quasi-static regime. In this regime, the inertial effects are negligible and contact forces between grains are balanced with self-weight and external load. In addition, grains are shown to form "force chains" in photoelastic experiments. Nevertheless, in rapid landslides and dry granular avalanches, some grains are highly agitated and grains interact with each other via frequent binary collisions instead of enduring contacts, which is termed a collisional regime by most researchers (Campbell 2006). Furthermore, the state that lies between the quasi-static regime and the collisional regime can be called an inertial regime, where the inertial effects are of the same magnitudes as the contact forces. It has been proved by both physical experiments and discrete element simulations that the Mohr–Coulomb friction angle becomes larger in both the inertial regime and the collisional regime (Midi 2004). From the energy perspective, it is easier to convert the mechanical energy of grains into the internal energy through collisions than through friction contacts.

SPH is a particle-based Lagrangian method (Monaghan 1992), where the continuum is represented by a large number of discrete particles. A number of researchers have improved its accuracy and stability (Liu and Liu 2010). SPH was initially used in astrophysics and fluid dynamics (Monaghan 1992; Liang 2010; Liang et al. 2010), and has also been employed in the study of non-Newtonian fluids (Shao and Lo 2003). Efforts have also been made in implementing Mohr-Coulomb type models in the SPH method to study slope stability (Fukagawa et al. 2011), large deformations of soil (Bui and Fukagawa 2008), bed scouring (Ulrich et al. 2013) and sediment flushing (Manenti et al. 2011).

Direct observations and detailed measurements of the dynamics of in-situ landslides and rockslides are scarce. To validate the Mohr-Coulomb model and to account for shear-rate dependence effect on the prediction of dry granular flows, this paper uses small-scale laboratory experiments of granular materials collapsing onto horizontal or inclined plates as benchmarks. The Smoothed Particle Hydrodynamic (SPH) method is utilised to numerically implement the Mohr-Coulomb model with and without considering the rate-dependence effect.

1 Mohr-Coulomb Model with the Shear-rate Dependence Effect

The mobilisation of granular materials has been extensively researched in the soil mechanics community. The Mohr-Coulomb model reads

$$\tau = c + \sigma \tan\phi \tag{1}$$

where τ is the shear strength, σ is the normal stress, c is the cohesion and ϕ is the internal friction angle. Additionally, $\tan\phi$ is called friction coefficient and can be denoted as μ. The critical state theory can describe not only the plastic deformation of soil but also the continuous flow of soil after failure with a set of unified equations. At the critical state, shear distortions occur without any further changes in the mean effective stress, deviatoric stress and volume fraction of solids. The ratio of the deviatoric stress to the mean effective stress at the critical state is a material parameter called the critical state frictional constant.

It has been observed in triaxial compression experiments that the critical state frictional constant and volumetric fraction of solids are shear-rate dependent (Namikawa 2001). Steady state shear flow experiments also confirm this observation. Both laboratory experiments (Hartley and Behringer 2003) and Discrete Element Method (DEM) simulations (Cruz et al. 2005) of the granular flows in simple configurations have been conducted to study this shear-rate dependence feature. The review paper of Midi (2004) gives a comprehensive summary of these results, based on which the inertial number is identified to represent the transition between quasi-static regime and inertial regime. When it is smaller than a specific value as in the quasi-static regime, the friction coefficient is constant. When the inertial number is larger than a specific value, as in the inertial regime,

the friction coefficient increases with shear rate, indicating a shear-rate dependence characteristic. A local rheology model has been proposed to capture the main features observed in these experiments. In all experiments mentioned above, shearing is only in one direction. Jop et al. (2006) generalised the rheology model into three-dimension, and demonstrated that the model successfully predicted the three-dimensional granular flow in a chute experiment with two rough walls. This model is used in this paper to account for the shear-rate dependence effect. The shear-rate dependent Mohr-Coulomb model can be expressed as

$$\tau_{ij}=\left(\mu_s+(\mu_\infty-\mu_s)\frac{1}{I_0/I+1}\right)P\frac{\dot{\gamma}_{ij}}{|\dot{\gamma}|} \qquad (2)$$

where τ_{ij} is the shear stress tensor, $\dot{\gamma}_{ij}$ is the shear rate tensor, $|\dot{\gamma}|$ is the second invariant of shear rate tensor $\dot{\gamma}_{ij}$, P is the local pressure. μ_s, μ_∞ and I_0 are free parameters. I is the inertial number as calculated by

$$I=\frac{|\dot{\gamma}|d_s}{\sqrt{P/\rho_s}} \qquad (3)$$

with ρ_s the density of grains and d_s the average diameter of grains.

The above model assumes that the stress tensor and shear rate tensor have the same principle directions. Lacaze and Kerswell (2009) proved this assumption by DEM simulations of axial symmetrical granular collapses and found that the principal axes of stress tensor and shear rate tensor are surprisingly well aligned, with 95% of the angle differences within 10°. The misalignment that does occur is invariably confined at the low-density free surface and near low-speed regions. The effective friction coefficient can be defined as

$$\mu_e=\left(\mu_s+(\mu_\infty-\mu_s)\frac{1}{I_0/I+1}\right) \qquad (4)$$

As we can see, when the shear rate $|\dot{\gamma}|$ is zero, then the inertial number is also zero and the effective friction coefficient is μ_s. Therefore, μ_s is called quasi-static friction coefficient. When the shear rate $|\dot{\gamma}|$ is very large and the inertial number approaches infinity, then the effective friction coefficient is μ_∞. Hence, μ_∞ is called the ultimate friction coefficient. In contrast, the conventional Mohr-Coulomb model reads

$$\tau_{ij}=\mu_s P\frac{\dot{\gamma}_{ij}}{|\dot{\gamma}|} \qquad (5)$$

where the effective friction coefficient is a constant.

The effective friction coefficient is an important parameter that influences the behaviour of granular flows. It represents the speed at which mechanical energy transforms into internal energy. The effective friction coefficient can increase from 0.23 at quasi-static regime to an ultimate value of 0.36 in plane shear tests (Midi 2004). Jop et al. (2006) reported the increase of the effective friction angle from 20° to 33° in his chute granular flow experiments. As can be seen, the magnitude of the increase in the effective friction coefficient is significant, and the influence of this increase on the idealised landslide phenomena is investigated herein.

The volumetric fraction of solids also depends on shear rate. The relation of volumetric fraction to the inertial number can also be constructed. Generally, the larger the inertial number, the smaller the volumetric fraction of solids. However, Forterre and Pouliquen (2008) reported that the variation of volumetric fraction is small in most granular flows and the incompressible assumption is reasonable. Because the incompressible assumption decouples the dilatancy equation and the friction equation, it greatly simplifies the model. Therefore, the incompressible assumption is made in this paper.

2 Smoothed Particle Hydrodynamics Method

Through kernel approximation and particle approximation, field variables and differentiation of field variables can be transformed into sum operations over neighbouring particles. For example, for a field viarable $f(\mathbf{x})$, the SPH estimate at position $\mathbf{x}_a$ can be expressed as

$$\langle f(\mathbf{x}_a)\rangle=\sum_{b=1}^{N}\frac{m_b}{\rho_b}f(\mathbf{x}_b)W(|\mathbf{x}_a-\mathbf{x}_b|,h) \qquad (6)$$

The SPH estimate of $\nabla f(\mathbf{x})$ at position $\mathbf{x}_a$ can be calculated as

$$\langle\nabla f(\mathbf{x}_a)\rangle=\sum_{b=1}^{N}\frac{m_b}{\rho_b}f(\mathbf{x}_b)\nabla W(|\mathbf{x}_a-\mathbf{x}_b|,h) \qquad (7)$$

where m_b is the mass of the particle positioned at

$\mathbf{x}_b$ and ρ_b is its density. On the right hand sides of these equations, the sum is for all neighbouring particles and $W(|\mathbf{x}_a-\mathbf{x}_b|,h)$ is the smoothing function. $W(|\mathbf{x}_a-\mathbf{x}_b|,h)$ can be denoted as W_{ab} for short and $\nabla W(|\mathbf{x}_a-\mathbf{x}_b|,h)$ can be expressed as $\nabla_a W_{ab}$ for short. The smoothing function is commonly an even function satisfying the renormalization condition and compact condition. In this study, the 2D cubic spline kernel is used. Hence, partial differential equations can be reduced into ordinary differential equations for transient problems. From now on, the bracket representing the SPH estimate of a variable will be dropped to avoid clutter in the expressions.

2.1 Incompressible SPH implementation

An incompressible SPH technique is used in this paper, in which the pressure projection method is implemented to impose the incompressibility constraint. Under the action of the pressure field alone, both linear momentum and angular momentum should be preserved. In order to ensure the conservation of angular momentum under the action of the shear stresses, a kernel correction procedure is adopted (Khayyer et al. 2009).

The technique consists of a predictor step and a corrector step. The first step is the integration in time considering only the gravity term and shear stress term in the momentum equation. The intermediate velocity and position of particle a are obtained as follows

$$\Delta\mathbf{v}_{a,1}=\left(\mathbf{g}+\frac{1}{\rho_a}\nabla\cdot\tau_a^t\right)\Delta t \tag{8}$$

$$\mathbf{v}_a^*=\mathbf{v}_a^t+\Delta\mathbf{v}_{a,1} \tag{9}$$

$$\mathbf{x}_a^*=\mathbf{x}_a^t+\frac{1}{2}(\mathbf{v}_a^t+\mathbf{v}_a^*)\Delta t \tag{10}$$

Here Δt is the time step. For particle a, $\mathbf{v}_a^*$ is the intermediate velocity, $\mathbf{x}_a^*$ is the intermediate position, $\mathbf{v}_a^t$, $\mathbf{x}_a^t$ and τ_a^t are the velocity, position and shear stress tensor, respectively, at the previous time step. The SPH formulation of equation (8) is

$$\Delta\mathbf{v}_{a,1}=\left(\mathbf{g}+\sum_{b=1}^{N}m_b\left(\frac{\tau_b^t}{\rho_b^2}+\frac{\tau_a^t}{\rho_a^2}\right)\cdot\nabla_a W_{ab}\right)\Delta t \tag{11}$$

Here, the stress is evaluated through a symmetric expression proposed by Monaghan (1992) rather than equation (7). Hence, the forces between two particles always obey the Newton's third law. Similar treatmentment is used in evaluting the pressure gradiant. No kernel correction is carried out to improve the consistency of the particle approximation in this study, so the evaluation of the stress terms is first-order accurate with regularly distributed particles, and less than first-order accurate with irregularly distributed particles. In Equation (11), ρ_a is the density of particle a at the previous time step, and it is calculated as

$$\rho_a=\sum_{b=1}^{N}m_b W_{ab} \tag{12}$$

Similarly, the intermediate density at particle a is calculated as

$$\rho_a^*=\sum_{b=1}^{N}m_b W_{ab}^*=\sum_{b=1}^{N}m_b W(|\mathbf{x}_a^*-\mathbf{x}_b^*|,h) \tag{13}$$

In the predictor step, incompressibility is not enforced. Then a corrector step is introduced to adjust the intermediate density to its assumed value. The correction to the velocity is obtained by considering the pressure term

$$\Delta\mathbf{v}_{a,2}=-\left(\frac{1}{\rho_a}\nabla p_a^{t+1}\right)\Delta t \tag{14}$$

Its SPH formulation is

$$\Delta\mathbf{v}_{a,2}=-\sum_{b=1}^{N}m_b\left(\frac{p_b^{t+1}}{\rho_b^2}+\frac{p_a^{t+1}}{\rho_a^2}\right)\nabla_a W_{ab}^*\Delta t \tag{15}$$

To revise the intermediate density to its initial constant value, the correction to the intermediate velocity must satisfy the following equation

$$\frac{1}{\rho_a}\frac{\rho_a-\rho_a^*}{\Delta t}+\nabla\cdot(\Delta\mathbf{v}_{a,2})=0 \tag{16}$$

Combining equation (14) and equation (16) yields the pressure Poisson equation

$$\nabla\cdot\left(\frac{1}{\rho_a^*}\nabla p_a^{t+1}\right)=\frac{1}{\rho_a}\frac{\rho_a-\rho_a^*}{\Delta t^2} \tag{17}$$

It is possible to construct the SPH Laplace operator by employing equation (7) twice. However, it is reported that this direct projection is sensitive to boundaries and often causes instability; hence Cummins and Rudman (1999) proposed an

approximate projection that is analogous to the approximation of the viscous diffusion term. The SPH formulation of the pressure Poisson equation is

$$\frac{1}{\rho_a}\frac{\rho_a-\rho_a^*}{\Delta t^2}=\nabla\cdot\left(\frac{1}{\rho_a^*}\nabla p_a^{t+1}\right)= \sum_{b=1}^{N} m_b \frac{8}{\left(\rho_a+\rho_b\right)^2}\left(p_a^{t+1}-p_b^{t+1}\right)\frac{\mathbf{x}_{ab}\cdot\nabla_a W_{ab}}{\left|\mathbf{x}_{ab}\right|^2+\eta^2} \quad (18)$$

where $\mathbf{x}_{ab}=\mathbf{x}_a-\mathbf{x}_b$ and η is a small value to always keep the denominator non-zero. Therefore, after the predictor step, this Poisson equation is solved based on the intermediate density to obtain the new pressure. For a SPH simulation involving N particles, there are N linear equations for the pressure distribution. The coefficient matrix of these coupled linear equations is a sparse matrix. Finally, the velocity and position at next time step is updated by

$$\mathbf{v}_a^{t+1}=\mathbf{v}_a^*+\Delta\mathbf{v}_{a,2}=\mathbf{v}_a^t+\Delta\mathbf{v}_{a,1}+\Delta\mathbf{v}_{a,2} \quad (19)$$

$$\mathbf{x}_a^{t+1}=\mathbf{x}_a^t+\frac{1}{2}(\mathbf{v}_a^t+\mathbf{v}_a^{t+1})\Delta t \quad (20)$$

2.2 Implementation of the Mohr-Coulomb model

The Mohr-Coulomb equation is implemented in the incompressible SPH code in the predictor step. At first, the local shear rate tensor of every particle is calculated. Based on the definition of shear rate

$$\dot{\gamma}_a^t=\left(\nabla\mathbf{v}^t+\left(\nabla\mathbf{v}^t\right)^T\right)_a \quad (21)$$

Its SPH formulation is obtained

$$\dot{\gamma}_a^t=\sum_{b=1}^{N}\frac{m_b}{\rho_b}\left[\left(\mathbf{v}_b^t-\mathbf{v}_a^t\right)\otimes\nabla_a W_{ab}+\nabla_a W_{ab}\otimes\left(\mathbf{v}_b^t-\mathbf{v}_a^t\right)\right] \quad (22)$$

Then, the shear rate $\left|\dot{\gamma}\right|$ is calculated from the shear rate tensor. For the conventional Mohr-Coulomb model, equation (5) is used to estimate local shear stress for every particle. For shear-rate dependent Mohr-Coulomb model, equation (2) is employed.

2.3 Boundary conditions

When updating the velocity and position of particles using equations (11) and (15), no special treatment is needed for free surface particles. For wall boundaries, the dummy particle method is adopted.

When solving the Poisson pressure equation, Neumann boundary condition is necessary for near-wall particles. In this paper, we follow the method proposed by Cummins and Rudman (1999). The Neumann condition is implemented with the assistance of virtual particles whose positions are dynamically determined by mirroring the interior fluid particles on the other side of the wall. For free surface particles, the pressure is assigned to zero. Therefore, correctly identifying free surface particles is of huge importance in solving the Poisson pressure equation. If an interior particle is mistakenly labelled as a free surface particle, then the whole solution is erroneous.

The basic idea behind identifying free surface particles is to take advantage of the particle deficiencies near the free surface. In other words, the following inequalities hold true for free surface particles

$$\sum_{b=1}^{N}\frac{m_b}{\rho_b}W_{ab}<1 \quad (23)$$

$$\sum_{b=1}^{N}\frac{m_b}{\rho_b}\nabla_a W_{ab}\neq 0 \quad (24)$$

For free surface particles, the left hand side of equation (23) is significantly smaller than 1 and the left hand side of equation (24) considerably deviates from 0. The free surface particles can be detected by calculating the estimated density via equation (12) (Khayyer et al. 2009). Marrone et al. (2010) proposed a more sophisticated method that employs the normal vector of free surface particles. In this study, a two-step free surface detection technique is employed based on the knowledge that, for a free surface particle, the normal vector of the free surface can be approximated by

$$\mathbf{n}=\frac{\sum_{b=1}^{N}\frac{m_b}{\rho_b}\nabla_a W_{ab}}{\left|\sum_{b=1}^{N}\frac{m_b}{\rho_b}\nabla_a W_{ab}\right|} \quad (25)$$

In the first step, the left hand side of equation (24) is computed for every particle and compared with a threshold. If it is greater than the threshold value, this particle can be regarded as a free surface

particle candidate. In order words, the following inequality is tested:

$$\sum_{b=1}^{N} \frac{m_b}{\rho_b} \nabla_a W_{ab} > \frac{m_a}{\rho_a} W_f \tag{26}$$

The larger the value of W_f, the more particles are eliminated in the first step. In addition, W_f also depends on the kernel function used.

Subsequently, equation (25) is exploited to evaluate the normal vector for every candidate particle. For a candidate particle a and one of its neighbouring particles b, $\mathbf{x}_{ab}$ is the vector pointing from particle a to b. The angle between $\mathbf{x}_{ab}$ and $\mathbf{n}$ is calculated for all neighbour particles of a. If there is one neighbour particle whose angle is smaller than a specified value, then particle a is not a free surface particle. In other words, the following inequality is tested.

$$\frac{\mathbf{n} \cdot \mathbf{x}_{ab}}{|\mathbf{x}_{ab}|} > \frac{\sqrt{2}}{2} \quad \text{for all b} \tag{27}$$

Only when inequalities (26) and (27) are both met will a particle be regarded to be at the free surface.

3 Application to the Collapse of Granular Columns

Recently, a number of studies were presented about the transient granular flows formed by the sudden release of vertical columns of grains on horizontal or inclined planes. These granular flows show similar characteristics to landslides. For example, they are unsteady flows and their free surface greatly changes with time. The inertial forces largely dominate frictional forces during the rapid movement. If the inclined slope angle is smaller than the internal friction angle, the grains will deposit on the slope; this process is characterised by the continuous deposition of grains on already stationary grains. So far, these experiments include axisymmetric collapses (Thompson and Huppert 2007) and planar collapses (Lube et al. 2005, 2011).

The high quality experimental results obtained by Lube et al. (2005, 2011) are used here as benchmark data for validating the numerical models. In these experiments, dry granular columns are initially contained in a rectangular box. The initial width and height of the columns are denoted as d_i and h_i respectively. The aspect ratio is h_i / d_i. In all experiments, the box is initially placed on the left of the domain. On the right side, there is a removable gate, followed by an inclined channel connected to the removable gate with an inclined angle denoted by θ. With regard to the final deposition shape, δd is the distance that the front has travelled along the slope to the right, and the final spread of the profile is defined as $d_\infty = \delta d + d_i / \cos\theta$. The final height of the assembly at the left wall is h_∞. Four kinds of granular materials (Coarse quartz sand, fine quartz sand, rice and sugar) are employed in the experiments. These materials have different average diameters, but they produce the same flow process and the same final deposition shape as they have almost identical quasi-static friction angle, which is the embankment angle of a granular pile resulting from slowly pouring grains from a small height onto a horizontal plane. The quasi-static friction angle provided by the experimenters is 31°, and the corresponding quasi-static friction coefficient μ_s is 0.6009. This value is used in the conventional Mohr-Coulomb model (5) and the shear-rate dependent Mohr-Coulomb model (2). The ultimate friction coefficient, μ_∞, is not provided by the authors. However, as reported in Jop et al. (2006) and Midi (2004), the ultimate friction angle is generally 10° larger than the quasi-static friction angle, then 0.8391 is chosen as the ultimate friction coefficient, and I_0 is set at 0.279 in shear-rate dependent Mohr-Coulomb model. In the experiments, columns were released in chutes 20 cm wide between two sidewalls. The samples were prepared with the same width, which is larger than the samples' length and height. Therefore, the friction of sidewalls is negligible and these experiments can be regarded to be two-dimensional. In all simulations, the fluid particles are initially arranged in a regular square lattice, with boundary particles added to form the wall and bed.

3.1 The numerical convergence study

To investigate the convergence of the SPH simulation, three test runs with different particle spacing were carried out to study the collapse of a column (d_i =0.083m and h_i =0.05m) onto a

horizontal ground. The conventional Mohr-Coulomb model is used in all three runs. These runs have particle numbers of 2065, 4150 and 8190, corresponding to particle spacing of $\sqrt{2}\times10^{-3}$ m, 1×10^{-3} m and $\sqrt{2}/2\times10^{-3}$ m, respectively.

One feature of granular flows is that grains are highly agitated near the front (Hutter et al. 1995), which is described as the saltating front by Lube et al. (2011). A region continuously occupied by grains follows the saltating front. The length of the saltating region increases with time and also with the basal inclination. When the flow comes to a halt, there is only one thin layer of grains at the front. In experiments, the front location is identified to be the position where half of the width of the chute is covered with one layer of grains. As the SPH method is particle-based, the computed front is also composed of one layer of particles, and the front position in this paper refers to the position of the particle that travels the shortest distance within this layer. Figure 1 shows the evolution of front positions with time in all three runs. It shows that the front position converges quickly at increasingly smaller particle spacing. When the number of particles increases from 2065 to 4150, the front position changes significantly between 0.12 s to 0.2 s. However, when the number of particles changes from 4150 to 8190, the two corresponding curves are very close.

At every step of calculation, the kinetic energy of all particles E_k, the gravitational potential energy of all particles E_g (the initial bottom of the column is chosen as the datum) and total mechanical energy E_m are evaluated.

$$E_k = \sum_i m_i |\mathbf{v}_i|^2 / 2 \tag{28}$$

$$E_g = \sum_i m_i g h_i \tag{29}$$

$$E_m = E_k + E_g \tag{30}$$

The evolution of these three kinds of energy for all three runs is presented in Figure 2. It can be seen that the potential energy decreases from the initial value of 1.62 Jm^{-1} to 1.21 Jm^{-1}, and the kinetic energy peaks at 0.07 Jm^{-1} at 0.08 s before approaching zero again when the granular flow comes to a stop. Following a similar procedure of Shao and Lo (2003), the order of the convergence speed is estimated to be 1.09 based on the total mechanical energy data, which confirms the

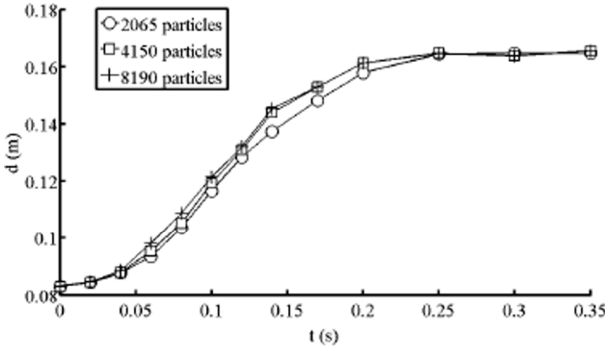

Figure 1 Dependence of the column front displacement on particle resolutions, horizontal bed, h_i = 0.05 m, d_i = 0.083 m, conventional Mohr-Coulomb model.

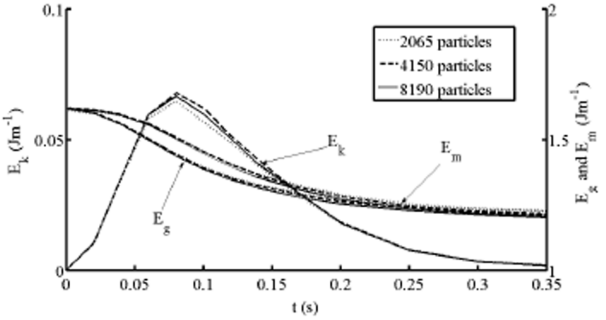

Figure 2 Evolution of the kinetic energy E_k, potential energy E_g and total energy E_m during the collapse, horizontal bed, h_i = 0.05 m, d_i = 0.083 m, conventional Mohr-Coulomb model.

conclusion by Liu and Liu (2010) that the SPH method has more than first order and less than second order accuracy. In the following studies, the granular assembly is composed of 5000 to 6000 particles, giving sufficiently small spacing.

3.2 Verification of the SPH simulations

Qualitative observations (Lube et al. 2005) in experiments reveal a strong dependence of the flow behaviour on the initial aspect ratio. Therefore, numerical experiments with a range of aspect

Table 1 The parameters of the four groups of numerical experiments

Group	d_i (m)	h_i (m)	θ (°)	M_C
A	0.083	0.05-0.166	0	Planar
B	0.048	0.0288-0.096	0	Axisymmetric
C	0.083	0.05	4.2-40	Planar
D	0.06	0.12	4.2-40	Planar

Notes: M_C=Manner of collapse

ratios (0.6, 1, 1.5 and 2) were carried out, when the ground surface is horizontal. They can be divided into two groups, with Group A referring to planar collapses and Group B referring to axisymmetric collapses. In addition, the slope of the ground also has a strong influence on the flow behaviour (Lube et al. 2011). Therefore, another two groups of simulations (group C and D) are conducted on slopes of different inclined angles (4.2°, 10°, 15°, 20°, 30°, 40°). Group C is the collapse of a shallow column (h_i / d_i =0.6) and Group D is the collapse of a tall column (h_i / d_i =2). A summary of the configurations of these tests is listed in Table 1. In the numerical analyses, two test runs were made for each scenario. One run used the conventional Mohr-Coulomb model (5), and the other run used the shear-rate dependent Mohr-Coulomb model (2) to evaluate the rate dependence effect.

An important feature of the collapse of granular columns is the evolution of the dynamic interface that separates the static region from the flowing region. The SPH simulations can reproduce this phenomenon faithfully. Initially, the interface appear to be a straight line intercepting the right gate at the bottom corner, and is inclined at 61° to the horizontal axis. Figures 3 and 4 show the evolution of velocity field for a shallow column ($h_i / d_i = 0.6$) and a

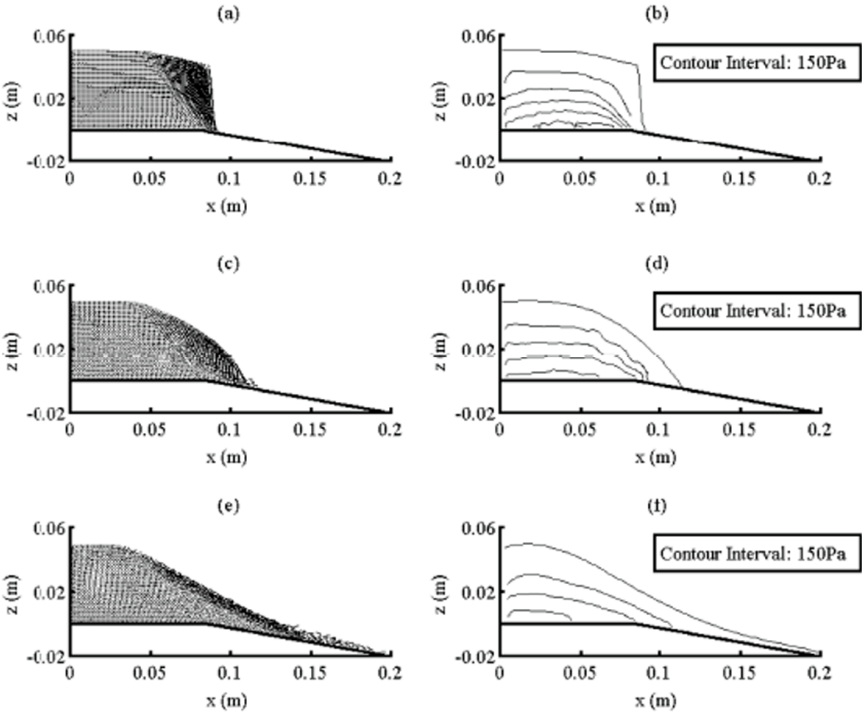

Figure 3 Velocity and pressure fields of a shallow column, 10° slope, h_i = 0.05 m, d_i = 0.083 m, shear-rate dependent Mohr-Coulomb model: (a-b) 0.05 s, (c-d) 0.1 s, (e-f) 0.25 s.

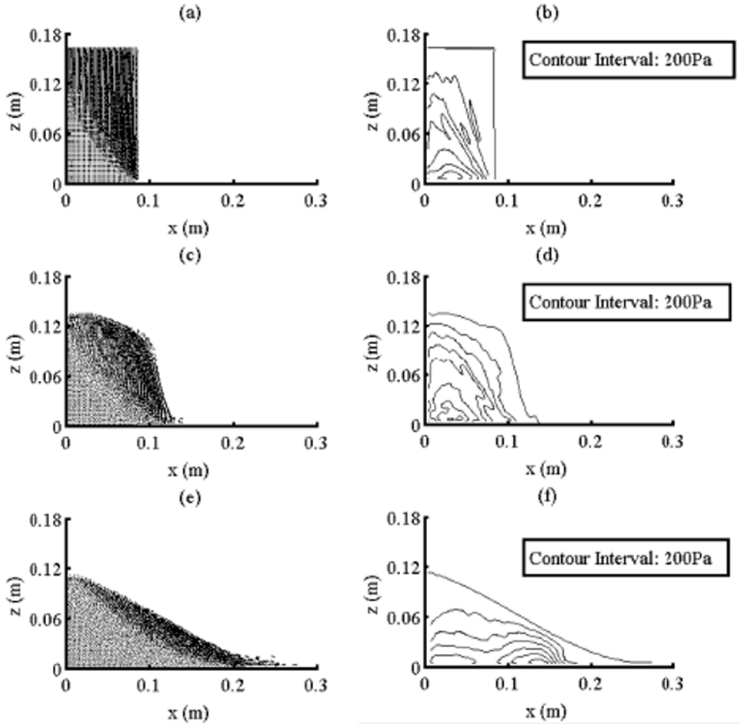

Figure 4 Velocity and pressure fields of a tall column, horizontal bed, h_i = 0.166 m, d_i = 0.083 m, shear-rate dependent Mohr-Coulomb model: (a-b) 0.02 s, (c-d) 0.12 s, (e-f) 0.25 s.

tall column ($h_i / d_i = 2$), respectively. In these two simulations, the shear-rate dependent Mohr-Coulomb model is used. Figure 3(a) and Figure 4(a) give the velocity fields shortly (0.05 s and 0.02 s) after the release, with Figure 3(b) and Figure 4(b) showing the corresponding pressure contours. Numerical calculation correctly predicts the same straight interfaces as the experimental observations. By comparing these interfaces at different times, we can conclude that the static region is growing with time and the interface shifts toward the free surface, thus the flowing region becomes thinner and thinner. When the interface coincides with the free surface, the granular flow comes to a stop completely.

In addition, a negligible part of the flowing region is seen to be in contact with the basal floor (Figure 3 and Figure 4). This explains why almost the same results are obtained for a diverse kind of basal materials. For this reason, the friction between granular materials and basal ground plays only a limited role in governing the collapse. As for the detailed dynamics of the flow, it was reported that the velocity profile at any position has the similar shape to those shown in Figure 5, which is composed of a static region at the bottom, a lower exponential-velocity region immediately above the static region, an upper linear-velocity-growth region, and a plug-flow region at the top. It can be seen that all the velocity profiles have a similar gradient in the linear-law region. Figure 5 shows that the SPH method successfully reproduces the expected velocity distribution inside the granular assembly.

The collapsing process depends strongly on the initial aspect ratio of the column. With regard to the final deposit shape, experiments show unique relationships between the non-dimensional final height (h_∞ / d_i) and the aspect ratio (h_i / d_i) and between the non-dimensional final front position ($\delta d / d_i$) and the aspect ratio (h_i / d_i). Figure 6 and Figure 7 summarize these relationships. For shallow initial piles, only grains above the fracture surface (slip surface) participate in the flow at the beginning, as seen in Figure 3(a). This interface intersects the top surface of the column. When the flow continues, this intersection point moves toward the vertical wall on the left, and more grains are eroded and get involved in the flow. For shallow piles, grains come to a stop

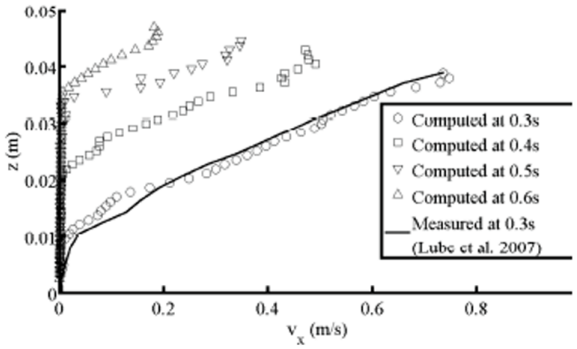

Figure 5 Velocity profiles over the depth at $x = d_i + (d_\infty - d_i)/3$, horizontal bed, h_i = 0.166 m, d_i = 0.083 m, shear-rate dependent Mohr-Coulomb model.

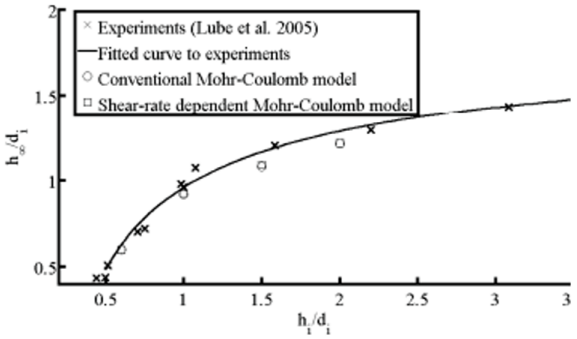

Figure 6 Variation of the non-dimensional final height (h_∞ / d_i) with the initial aspect ratio (h_i / d_i), horizontal bed

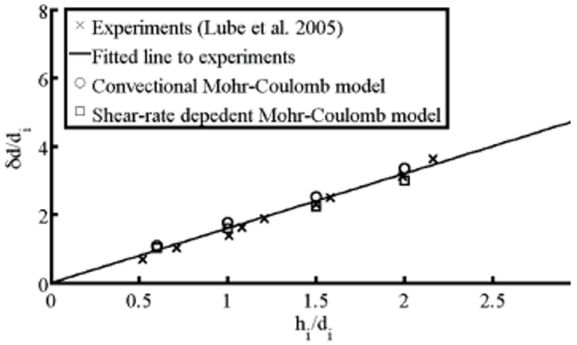

Figure 7 Variation of the non-dimensional final front displacement ($\delta d / d_i$) with the initial aspect ratio (h_i / d_i), horizontal bed

completely before this intersection point reaches the left vertical wall. Therefore, for low aspect ratio columns, the height of the final profile is equal to initial height ($h_\infty = h_i$). Hence, the non-dimensional height (h_∞ / d_i) linearly increases with the aspect ratio (h_i / d_i), as shown in the left part of Figure 6. Whereas, at larger aspect ratios, both the experimental results and the predictions indicate

that the final height gradually plateau. In contrast, Figure 7 shows that the relationship between the non-dimensional maximum front displacement always grows linearly with the aspect ratio. Figures 8 and 9 compare the final shape obtained in the experiments and the results extracted from SPH the simulations. It can be seen that the conventional Mohr-Coulomb model and shear-rate dependent Mohr-Coulomb model give similar results, and they both overestimate the volume of grains participating in the flow, which leads to more grains being eroded at the top surface. This is because these two models are only suitable for modelling the mechanics of the granular materials after failure. The mechanical behaviour before failure is more complex. For shallow columns, a small number of grains first participate in the flow and then quickly stop, for which the influence of plastic behaviour before the failure is not negligible. As for the dynamics of tall columns there is a critical height, above which the grains move like a free fall at first, as seen in Figure 4(a). The grains between the critical height and the dynamic interface move outwards. The eventual deposition takes the shape of a wedge, but there is no flat top on the left of the collapsed column when the aspect ratio is large, which leads to a final height being much smaller than the initial height. Therefore, the relation of h_∞ / d_i with h_i / d_i is strongly nonlinear at large aspect ratios. It is concluded from Figures 6-9 that, as far as the height of the final shape is concerned, the conventional Mohr-Coulomb model and the shear-rate dependent Mohr-Coulomb model give almost identical results and agree with experiments well.

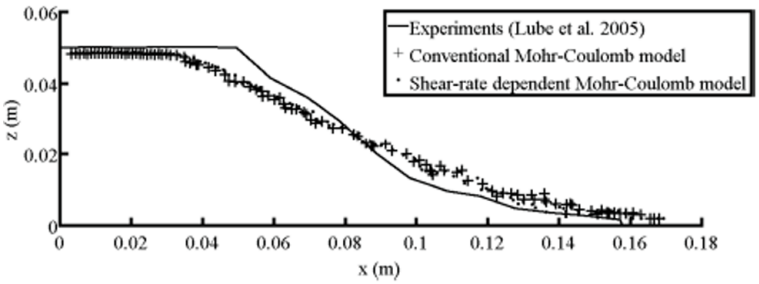

Figure 8 Final profile of a shallow column, horizontal bed, h_i = 0.05 m, d_i = 0.083 m.

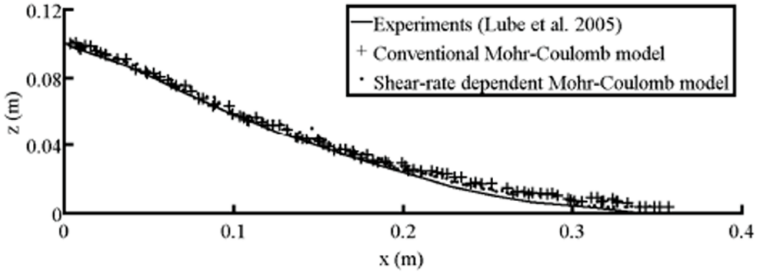

Figure 9 Final profile of a tall column, horizontal bed, h_i = 0.166 m, d_i = 0.083 m.

With regard to the final front position, Figure 7 gives the results obtained by SPH simulations for both models and the corresponding experimental measurements. It can be seen that, for shallow columns, both models produce identical estimation of the front position. However, when the aspect ratio increases, which means that more grains get involved in the deformation, the shear-rate dependent Mohr-Coulomb model gives a smaller estimate than the conventional Mohr-Coulomb model. However, the discrepancy is not big, and both models compare favourably with the measurements.

3.3 The rate-dependence effect on runout

It is obvious that when granular columns are released onto inclined channel planes, the grains travel further, and take a longer time to come to rest. Figure 10 depicts the evolution of the front positions after releasing a shallow column of grains onto slopes of different inclined angles, the conditions of which are listed in the Group C numerical experiments. When the inclined angle is larger than the frictional angle, the grains will never stop, but travel faster and faster on the slope, as indicated by curves for 30° and 40° slopes in Figure 10. There are surprising changes of curve gradient for ground slopes of 20° and 30° between 0.4 s and 0.45 s in Figure 10. According to the curve for 20°, the flow seems to come to a pause at 0.4 s, but then travels a bit further before a final stop after 0.45 s. According to the curve for 30°, the flow seems about to stop at 0.4 s, but then starts to accelerate after 0.45 s. This is because for

a shallow column collapsing onto mild slopes, grains would come to a complete stop before the erosion line reaches the vertical wall. However, for a collapse onto steep slopes (larger than 20°), the erosion line reaches left wall between 0.4 s and 0.45 s, which causes a slight change in the trend of the curve.

Figure 11 shows the relationship between the non-dimensional final front position and the inclined angle of the slope in conditions tested in Groups C and D. Experimental results are also included. The upper solid line is the experimental result for a tall column and the lower solid line is for a shallow column. The figure shows that, for a shallow collapse onto slopes less than 20°, both models obtain similar results that agree equally well with experimental results. When the slope increases beyond 20°, the conventional Mohr-Coulomb model overestimates the front position by more than 40% of the experimental value. In contrast, the shear-rate dependent Mohr-Coulomb model gives only a 10% overestimate. For tall columns, similar results can be obtained, but the predicted results by these two models show clear discrepancy even when the slope is small. Although the shear-rate dependent Mohr-Coulomb model obtains better result, it still slightly overestimates the front position by around 10% on steep slopes, which can be attributed to the inaccuracy of the ultimate friction coefficient chosen in the simulation.

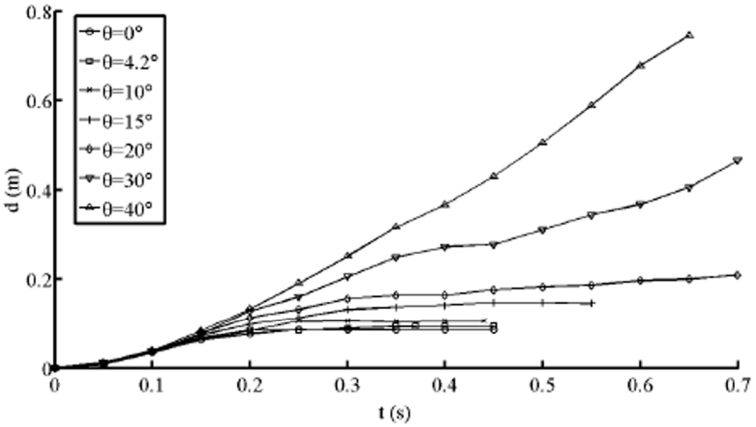

Figure 10 Shallow column front advancement, h_i = 0.05 m, d_i = 0.083 m, shear-rate dependent Mohr-Coulomb model.

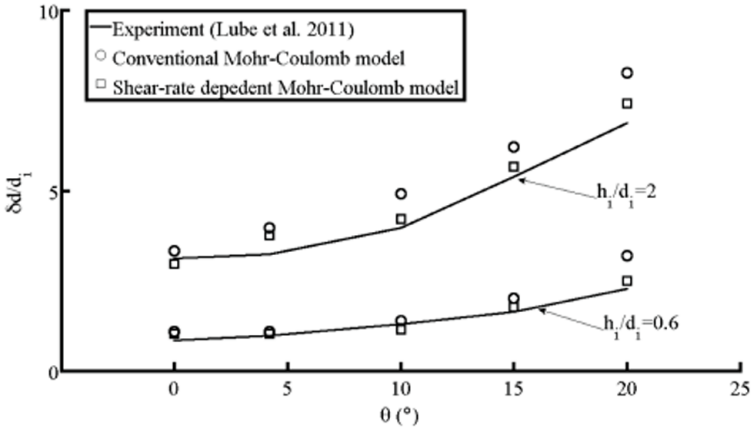

Figure 11 Variation of the non-dimensional final front displacement with the bed slope.

The granular flow process consists of three stages, the mobilization stage, the flow stage, and the deposition stage. During mobilization stage and deposition stage, the grains are in a quasi-static regime and the effective frictional coefficient is small. During the flow stage, grains are agitated and local shear rates are large enough to see an apparent increase in the effective frictional coefficient. The conventional Mohr-Coulomb model overestimates the runout and the duration of the collapse. When the columns are released onto gradual slopes, the total collapse time is small. Therefore, the time in flow stage is relatively short and the influence of rate dependence effects is negligible. In contrast, when the columns are released onto steep slopes, the flow stage constitutes a significant part of the total process, and the influence of rate dependence is important. In addition, when the aspect ratio is larger, the depth of granular materials above the interface is larger and the static pressure at the interface is also larger. As the shear stress depends on the pressure in Mohr-Coulomb type equations, the increased frictional angle owing to the rate dependence effect is amplified by the large pressure. Consequently, we define a non-dimensional parameter for measuring the importance of rate dependence

effect.

$$b = \frac{d_\infty / d_i}{h_\infty / d_\infty} \tag{31}$$

The denominator is the final aspect ratio, which represents the magnitude of mean pressure at dynamic interface. The numerator represents the distance that the front has travelled. Therefore, for a shallow column, the grains should travel long enough to make b big enough such that the rate dependence effect comes into play. All the b values are calculated based on the experimental results and are shown in Table 2. From these data, a critical value $b_c \approx 6$ can be chosen. For the collapse of rectangular columns, when the calculated b is larger than 6, the rate dependence effect cannot be neglected. For a collapse along slopes steeper than internal friction angle, d_∞ is infinite. Consequently, b is infinite and the rate dependence effect is not negligible.

The evolution of mechanical energy has also been examined at large slope angles. Figure 12 and Figure 13 show the evolution of the kinetic energy, the gravitational potential energy and the total mechanical energy for the collapse of tall columns along a 20° slope and a 40° slope, respectively. For slopes smaller than the internal friction angle, the kinetic energy predicted by both models comes to a peak before declining to zero at the end. The final mechanical energy predicted by the shear-rate dependent Mohr-Coulomb model is slightly larger, which agrees with the above conclusion that the front travels a shorter distance. Therefore, grains come to a stable state with less mechanical energy dissipated into internal energy. When the slope is larger than the internal friction angle, the shear-rate dependent Mohr-Coulomb model also predicts a higher mechanical energy, and the difference between the two models becomes larger and larger. In addition, the conventional Mohr-Coulomb model overestimates kinetic energy, but underestimates the potential energy, with the errors increasing with time.

4 Conclusions

This paper presents the application of an incompressible SPH method to the collapse of dry granular columns. A two-step detection technique is proposed to accurately identify the free surface particles. The shear rate tensor is evaluated by summing up the velocity information of neighbour particles in the SPH formulation. The local shear stress is calculated from the Mohr-Coulomb type equations.

The convergence study shows that this algorithm converges rapidly, with a speed between the first order and second order schemes. Then, this algorithm is verified against column collapse experiments. All the key features can be successfully reproduced by the Mohr-Coulomb type models, such as the saltating front, distinctive dependence of the flow behaviour on the initial aspect ratio of the column, the evolution of the dynamic interface demarcating the static region

Table 2 The values of the non-dimensional parameter b in different cases

	0°	4.2°	10°	15°	20°
$h_i / d_i = 0.6$	1.17	1.59	2.74	4.38	8.54
$h_i / d_i = 2$	4.93	5.28	7.97	14.56	23.65

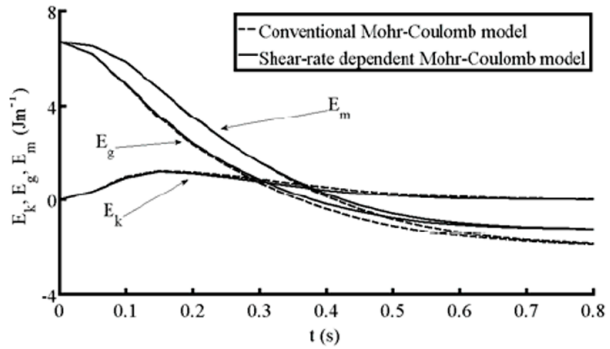

Figure 12 Evolution of the kinetic energy E_k, potential energy E_g and total energy E_m of a tall column, 20° slope, h_i = 0.12 m, d_i = 0.06 m.

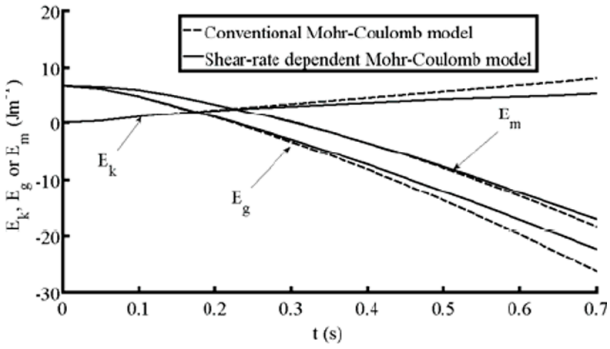

Figure 13 Evolution of the kinetic energy E_k, potential energy E_g and total energy E_m of a tall column, 40° slope, h_i = 0.12 m, d_i = 0.06 m.

and the flow region, and the velocity distribution.

The conventional Mohr-Coulomb model is compared with the shear-rate dependent Mohr-Coulomb model, especially concerning the final shape of the deposition. It is found that the rate dependence effect is negligible for the shallow granular flow along mild slopes. When the inclined ground steepens or the aspect ratio of granular column increases, the rate dependence effect becomes more important. A non-dimensional parameter is defined to measure the significance of rate dependence effect. When this parameter is larger than a critical value of 6, the rate dependence effect is not negligible.

Acknowledgements

The research is supported by the National Natural Science Foundation of China (Grant No. 51479111) and the Non-profit Industry Financial Program of the Ministry of Water Resources (Grant No. 201401027). We also thank the Raymond and Helen Kwok Scholarship of Jesus College, University of Cambridge.

References

Bui H, Fukagawa R (2008) Lagrangian meshfree particles method (SPH) for large deformation and failure flows of geomaterial using elastic–plastic soil constitutive model. International Journal for Numerical and Analytical Methods in Geomechanics 32(12):1537-1570. DOI:10.1002/nag

Campbell CS (2006) Granular material flows – An overview. Powder Technology 162(3):208-229. DOI:10.1016/j.powtec.2005.12.008

Cruz FD, Emam S, Prochnow M, Roux J, Chevoir F (2005) Rheophysics of dense granular materials: Discrete simulation of plane shear flows. Physical Review E 72(021309): 1-17. DOI:10.1103/PhysRevE.72.021309

Cummins SJ, Rudman M (1999) An SPH Projection Method. Journal of Computational Physics 152(2): 584-607. DOI: 10.1006/jcph.1999.6246

Forterre Y, Pouliquen O(2008) Flows of Dense Granular Media. Annual Review of Fluid Mechanics 40(1): 1-24. DOI: 10.1146/annurev.fluid.40.111406.102142

Fukagawa R, Sako K, Bui HH, Wells JC (2011) Slope stability analysis and discontinuous slope failure simulation by elasto-plastic smoothed particle hydrodynamics (SPH). Géotechnique 61(7): 565-574. DOI:10.1680/geot.9.P.046

Hartley RR, Behringer RP (2003) Logarithmic rate dependence of force networks in sheared granular materials. Nature 421(6926): 928-31. DOI:10.1038/nature01394

Jop P, Forterre Y, Pouliquen O(2006) A constitutive law for dense granular flows. Nature 441(7094): 727-30. DOI: 10.1038/nature04801

Khayyer A, Gotoh H, Shao S (2009) Enhanced predictions of wave impact pressure by improved incompressible SPH methods. Applied Ocean Research 31(2): 111-131. DOI: 10.1016/j.apor.2009.06.003

Lacaze L, Kerswell R (2009) Axisymmetric Granular Collapse: A Transient 3D Flow Test of Viscoplasticity. Physical Review Letters 102(10): 108305. DOI:10.1103/PhysRevLett.102.108305

Liang D (2010) Evaluating shallow water assumptions in dam-break flows. Proceedings of the ICE - Water Management 163(5): 227-237. DOI:10.1680/wama.2010.163.5.227

Liang D, Thusyanthan I, Madabhushi SPG and Tang H (2010) Modelling solitary waves and its impact on coastal houses with SPH method. China ocean engineering 24(2): 353-368

Liu MB, Liu GR (2010) Smoothed Particle Hydrodynamics (SPH): an Overview and Recent Developments. Archives of Computational Methods in Engineering 17(1): 25-76. DOI: 10.1007/s11831-010-9040-7

Lube G, Huppert H, Sparks R, Freundt A (2005) Collapses of two-dimensional granular columns. Physical Review E 72(4): 1-10. DOI: 10.1103/PhysRevE.72.041301

Lube G, Huppert HE, Sparks RSJ, & Freundt, A. (2011) Granular column collapses down rough, inclined channels. Journal of Fluid Mechanics 675(2011): 347-368. DOI:10.1017/jfm.2011.21

Manenti S, Sibilla S, Gallati M (2011) SPH simulation of sediment flushing induced by a rapid water flow. Journal of Hydraulic Engineering 138(3): 272-284. DOI:10.1061/(ASCE)HY.1943-7900.0000516.

Midi GDR (2004) On dense granular flows. The European Physical Journal. E, Soft Matter 14(4): 341-65. DOI:10.1140/epje/i2003-10153-0

Monaghan J (1992) Smoothed Particle Hydrodynamics. Annual Review of Astronomy and Astrophysics 30(1): 543-574. DOI:10.1146/annurev.astro.30.1.543

Namikawa T (2001) Delayed plastic model for time-dependent behaviour of materials. International Journal for Numerical and Analytical Methods in Geomechanics 25(6): 605-627. DOI:10.1002/nag.144

Savage S, Hutter K (1989) The motion of a finite mass of granular material down a rough incline. Journal of Fluid Mechanics 199: 177-215. DOI: 10.1017/S0022112089000340

Shao S, Lo EYM (2003) Incompressible SPH method for simulating Newtonian and non-Newtonian flows with a free surface. Advances in Water Resources 26(7): 787-800. DOI: 10.1016/S0309-1708(03)00030-7

Thompson EL, Huppert HE (2007) Granular column collapses: further experimental results. Journal of Fluid Mechanics 575: 177. DOI:10.1017/S0022112006004563

Ulrich C, Leonardi M, Rung T (2013) Multi-physics SPH simulation of complex marine-engineering hydrodynamic problems. Ocean Engineering 64: 109-121. DOI: 10.1016/j.oceaneng.2013.02.007